Supporting Information

Boosted electrochemical ammonia synthesis by metallic transition metal dichalcogenide quantum dots

Jian Zhang,[a,b] Chongyi Ling,[c] Wenjie Zang,[d] Xiaoxia Li,[b] Shaozhuan Huang,[b] Xueliang Li,[b] Dong Yan,[b] Zongkui Kou,[d] Lei Liu,[a] Jinlan Wang,[c] Hui Ying Yang*[b]

[a]Key laboratory of Material Chemistry for Energy Conversion and Storage, School of Chemistry and Chemical Engineering, Huazhong University of Science and Technology, Wuhan 430074, PR China

[b]Pillar of Engineering Product Development, Singapore University of Technology and Design, 8 Somapah Road, Singapore 487372, Singapore

[c]School of Physics, Southeast University, Nanjing 211189, P. R. China

[d]Department of Materials Science and Engineering, National University of Singapore, 117574, Singapore.

*Corresponding author.

E-mail address: yanghuiying@sutd.edu.sg (H.Y. Yang).

Materials and Methods

Chemicals.

Molybdenum powder (~22 mesh, 99.9975%, Puratronic®), selenium shots (1-3 mm, 99.999%, Puratronic®), n-Butyllithium solution (2.0 M in cyclohexane), n-hexane (anhydrous, 95%) and anhydrous sodium sulfate (Na_2SO_4), sulfuric acid (H_2SO_4) ammonium chloride (NH_4Cl), Hydrazine hydrate ($N_2H_4 \cdot H_2O$), dimethylaminobenzaldehyde ($C_9H_{11}NO$), sodium citrate dehydrate ($C_6H_5Na_3O_7 \cdot 2H_2O$), sodium nitroferricyanide dehydrate ($C_5FeN_6Na_2O \cdot 2H_2O$), and sodium hypochlorite solution (NaClO) were purchased from Alfa Aesar (USA). The high-purity of nitrogen (N_2, 99.9999%) and purified Argon (Ar, 99.99%) were

purchased from Leeden National Oxygen Ltd. in Singapore. Ethanol (99.9%) and acetone (Tech Grade) were purchased from Merck (Germany). The Milli-Q water used in experiments was obtained in the Milli-Q System (USA).

Preparation of $MoSe_2$ QDs

First, the 2H-phase layered bulk crystal $MoSe_2$ (**Fig. S**1a) was synthesized by combining chemical vapor transport (CVT) technique method. And then, the obtained bulk $MoSe_2$ was ground into small-sized crystals by a dry ball milling process under inert atmosphere with a Mixer Mill machine. A certain amount of $MoSe_2$ was put into grinding jar with four zirconia grinding balls. The grinding process was conducted under a vibrational frequency for five hours. The size of $MoSe_2$ layered bulk material decreased from tens of micrometers to about one micrometer or even smaller (**Fig. S1b**). After long-term high-energy ball milling, the obtained $MoSe_2$ powder was immersed into n-butyllithium solution (in cyclohexane) and then kept undisturbed for three days to allow the Li fully intercalated into the crystals. The upper solution of n-butyllithium was then removed carefully. Thereafter, the Li-intercalated powder was washed three times with n-hexane by centrifuge and then sonicated in the water. The obtained suspension was centrifuged at 12,000 rpm for 20 min to remove the small-sized $MoSe_2$ nanosheets. And then, the product was washed three times with Milli-Q water using Millipore ultrafiltration tubes. After freeze drying, the final product of $MoSe_2$ QDs was obtained.

Preparation of MoS_2, WSe_2, WS_2, $NbSe_2$ QDs

The Preparation process of MoS_2, WSe_2, WS_2, $NbSe_2$ QDs was similar as that of $MoSe_2$ QDs. Briefly, the bulk MoS_2, WSe_2, WS_2, $NbSe_2$ QDs were successively subjected to ball milling (5 hours), n-butyllithium immersion (3 days), sonication and high-speed centrifugal separation, the corresponded MoS_2, WSe_2, WS_2, $NbSe_2$ QDs were obtained. Noted that the ball milling process of the bulk $NbSe_2$ were underwent to Argon gas atmosphere to avoid the oxidation of the materials.

Characterization

The obtained $MoSe_2$ QDs suspension was dropped onto an ultrathin carbon-

coated holey copper grid for TEM characterization, onto clean Si substrates for Raman and XPS characterizations, and onto a clean mica substrate for AFM characterization. Transmission electron microscopy (TEM) images and energy dispersive X-ray spectroscopy (EDS) were recorded with JEOL-2100F at an acceleration voltage of 200 kV. Aberration-corrected scanning transmission electron microscopy (STEM) image was obtained on a JEOL ARM200F (JEOL, Tokyo, Japan) operated at 200 kV with cold field emission gun and double hexapole Cs correctors (CEOS GmbH, Heidelberg, Germany). Scanning electron microscopy (SEM) images were obtained using a field emission scanning electron microscope (SEM, JEOL JSM-7600F). Powder X-ray diffraction (XRD) was conducted using a Siemens D-500 X-ray diffractometer (Bruker AXS, Inc., Madison, USA). Atomic force microscopy (AFM, Cypher, Asylum Research, USA) was used to characterize the thickness of $MoSe_2$ QDs in tapping mode in air. Ultraviolet-visible (UV-vis) absorption spectrum was recorded on a UV-2700 (Shimadzu) with QS-grade quartz cuvettes (111-QS, Hellma Analytics) at room temperature. X-Ray photoelectron spectroscopy (XPS) measurements were performed using Kratos Axis-ULTRA X-ray photoelectron spectroscopy instrument equipped with a monochromatic Al Kα (1486.7 eV) X-ray source with emission of 10 mA and anode HT of 15 KV. Raman measurements were carried out on a triple grating (1800 g/mm) spectrometer (Horiba-JY T64000). A solid state laser (λ = 532 nm) was used to excite the sample. The backscattered signal was collected through a 50× long focus objective lens. Electron paramagnetic resonance (EPR) spectra were obtained using Bruker EMXnano wave spectrometer at room temperature. N_2 temperature programmed desorption (N_2-TPD) measurements were collected using a TP-5076 multiple adsorption instrument. The measured material was first pretreated with pure He at a flow rate of 30 mL·min−1 at 200 °C for 30 min, followed by cooling down to room temperature in the same atmosphere and then dosed with pure N_2. To remove residual N_2, the catalyst was purged with pure He at a flow rate of 30 mL·min−1 for 30 min. The N_2-TPD measurement was subsequently performed with the heating rate of 10 °C·min−1 in pure He.

Electrochemical NRR measurements

Electrochemical measurements for NRR were conducted by using an electrochemical workstation with a three-electrode system consisting of counter electrode (graphite rod), working electrode and reference electrode (Ag/AgCl/saturated KCl) at ambient conditions (room temperature and pressures). The working electrode was prepared by successively drop-casting samples and Nafion solutions onto the porous carbon paper. The effective surface area of all the applied electrodes was 0.2 cm^{-2}. The loading amount of all the catalysts was 0.02 mg on the working electrode. The N_2 reduction was carried out in a two-compartment electrochemical cell that was connected by an inverted U-type salt bridge (filled by saturated potassium chloride and agar, **Fig. S6**). Notably particularly, to avoid introducing any impurities, the feeded gases (N_2 and Ar_2) were purified by a home-made filtration system that in turn contained 0.1 M H_2SO_4 solution and pure water **(Fig. S6**) before the electrochemical reaction. The electrochemical NRR was mainly investigated by cyclic voltammetry (CV), linear sweep voltammetry (LSV), chronoamperometry (CA) and electrochemical impedance spectroscopy (EIS). All the measurements were carried out in the N_2-saturated 0.5 M Na_2SO_4 electrolyte, which was purged with N_2 gas (99.99%) for 30 min to remove residual air before the test. As control experiments, open-circuit potential tests in N_2-saturated 0.5 M Na_2SO_4 electrolyte, potentiostatic measurements in Ar-saturated 0.5 M Na_2SO_4 electrolyte, CA measurements with pure carbon paper electrode in N_2-saturated 0.5 M Na_2SO_4 electrolyte were all performed. The electrochemical active surface area (ECSA) of the catalysts was carried out from the double layer capacitance (C_{dl}). Noted that the catalysts were loaded on the glass carbon for ECSA measurements. All the presented current density was normalized to the geometric surface area. All of the potentials were transformed to the RHE scale according to the following equation,

$$E_{RHE} = E_{Ag/AgCl} + 0.1989 + 0.059 \cdot pH$$

Quantification of ammonia and hydrazine

The concentration of produced ammonia was measured by the indophenol blue method[1]. Typically, 2 mL electrolyte was obtained from the cathodic chamber and mixed with 25 μL oxidizing solution containing NaClO (ρCl = 4–4.9) and NaOH (0.75 m), 250 μL coloring solution containing 0.4 m $C_7H_6O_3$ and 0.32 m NaOH, and 25 μL catalyst solution (1 wt% $Na_2[Fe(CN)_5NO]$). After being kept at ambient conditions for 2 h in darkness, the absorption spectra of the aforementioned solution were acquired with an UV-Vis spectrophotometer. The concentration of formed indophenol blue was calculated by using the absorbance at 665 nm. The concentration-absorbance curve was calibrated by using a series of standard ammonia chloride solution with different concentrations. The fitting curve (Fig. S3, y =0.0113x + 0.173, R^2 = 0.999) shows good linear relation of absorbance value with NH3 concentration by three times independent calibrations.

The concentration of produced hydrazine was measured by the Watt and Chrisp method[1]. Firstly, the colour reagent was prepared by mixing *p*-dimethylaminobenzaldehyde (0.599 g), HCl (12 M, 3 mL) and ethanol (30 mL). After that, 1 mL of the as-prepared colour reagent was mixed with 1 mL of the 0.5 M Na_2SO_4 electrolyte solution that were collected after the NRR test. After being stirred at ambient conditions for 10 min, the absorption spectra of the aforementioned solution were acquired with an UV-Vis spectrophotometer. The absorbance of the resulting solution was measured at the wavelength of 455 nm. The concentration-absorbance curve was calibrated by using a series of standard hydrazine monohydrate solution with different concentrations (Fig. S4, y =0.021x + 0.09, R^2 = 0.999).

NRR performance evaluations

Faradaic efficiency (FE) and the ammonia yield rate (Rm). The Faradaic efficiency was calculated from the charge consumed for NH_3 production and the total charge passed through the electrode according to the following equation,

$$FE = \frac{3F \cdot C_{NH_3} \cdot V}{Q}$$

The ammonia yield rate (R_m) was estimated as follows,

$$R_m = \frac{17 \cdot C_{NH_3} \cdot V}{m \cdot t}$$

where C_{NH3} is the measured concentration of produced NH_3 (mol L^{-1}), Q is the total charge passed through the electrode (C), F is the Faraday constant (96500 C mol^{-1}), V is the volume of electrolyte (L, V = 0.04 L in this work), m is the loading amount of catalysts on the working electrode (mg, m = 0.02 mg in this work) and t is the reaction time (h, t = 2 h in this work).

Computational Details

Spin-polarized density functional theory (DFT) calculations were carried out by using Vienna ab initio simulation package (VASP).[2] Projector augmented wave (PAW)[3] method was adopted to describe the ion-electron interactions. The generalized gradient approximation in the Perdew-Burke-Ernzerhof (PBE) form[4] were used, and a cut-off energy of was set to 400 eV for plane-wave basis. The convergence criterion was set to 0.01 eV/Å and 10^{-5} eV for the residual force and energy, respectively. An infinite stripe model was used to investigate the activity of the edge and the Brillouin zones were sampled by a Monkhorst-Pack k-point mesh with a 5 × 1 × 1 kpoint grid. To avoid periodic interactions, a vacuum space of 20 Å was used. The free energy change (ΔG) of each elementary reaction is calculated as

$$\Delta G = \Delta E + \Delta E_{ZPE} - T\Delta S$$

where ΔE is the electronic energy difference directly obtained from DFT calculations, ΔE_{ZPE} is the change in zero-point energies, T is the temperature and ΔS is the entropy change.

Figures

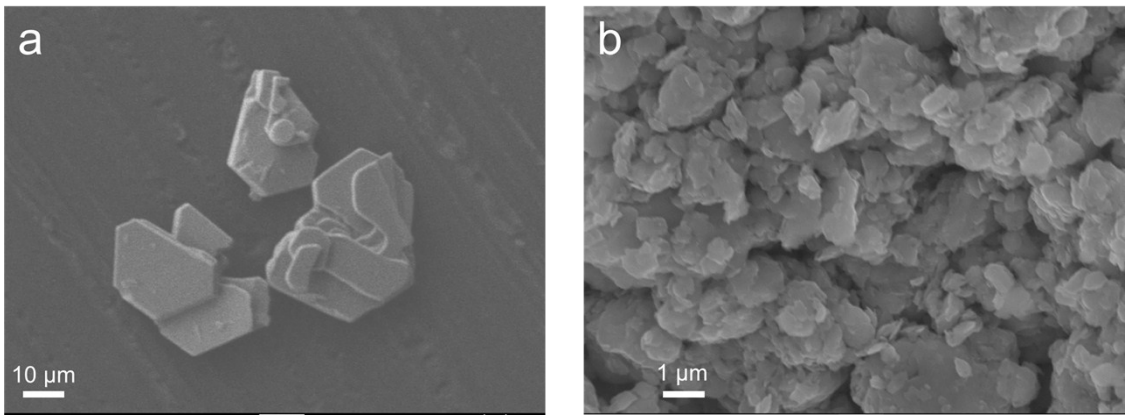

Fig. S1 SEM image of $MoSe_2$ (a) before and (b) after ball-milling.

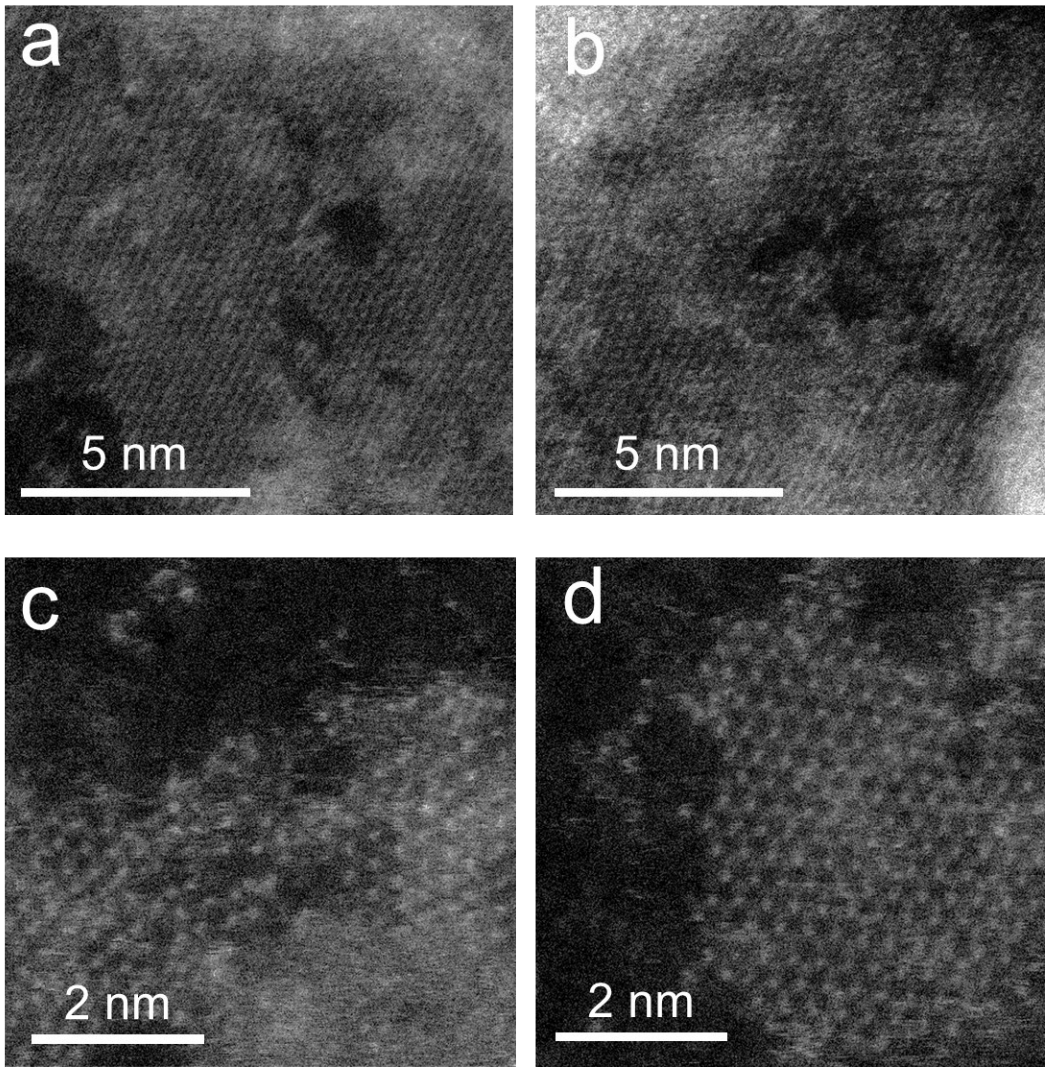

Fig. S2 (a-d) STEM image of 1T-$MoSe_2$ QDs.

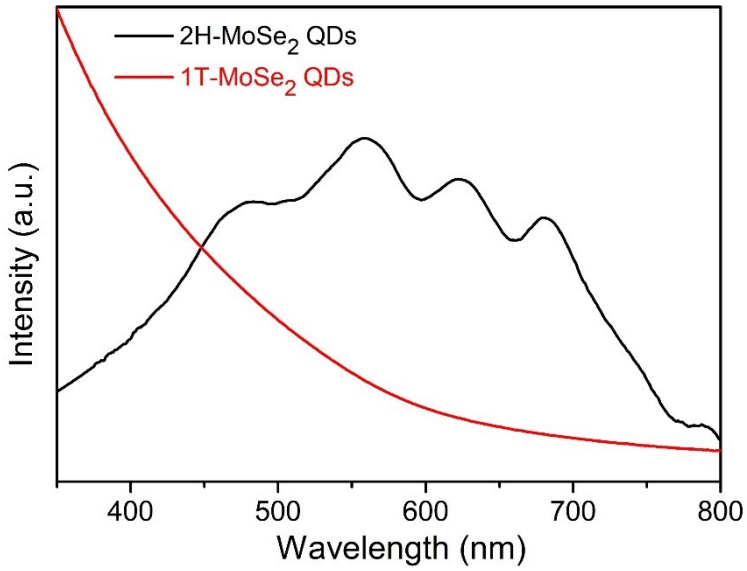

Fig. S3 UV-vis spectrum of 2H- and 1T -MoSe2 QDs.

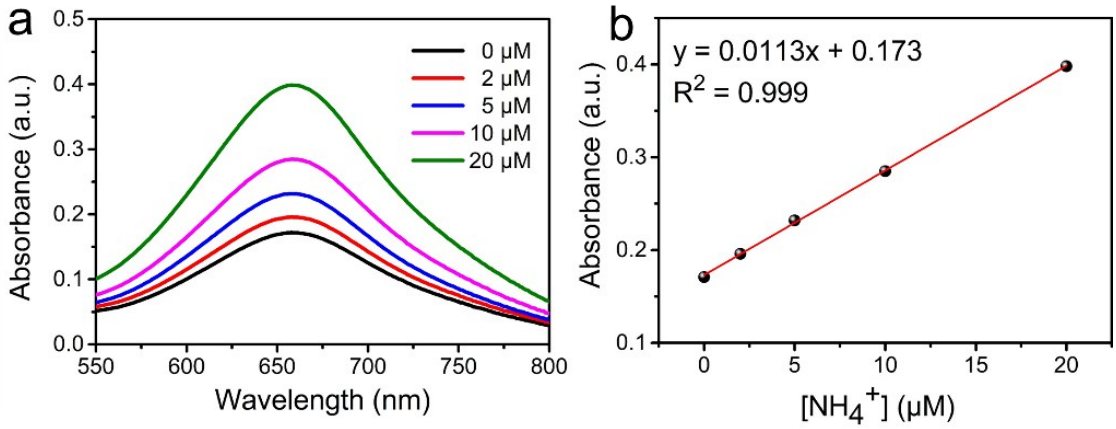

Fig. S4 (a) UV-Vis absorption spectra of indophenol assays with NH4+ ions after incubation for 2 h at room temperature; (b) calibration curve used for estimation of NH_3 by NH4+ ion concentration.

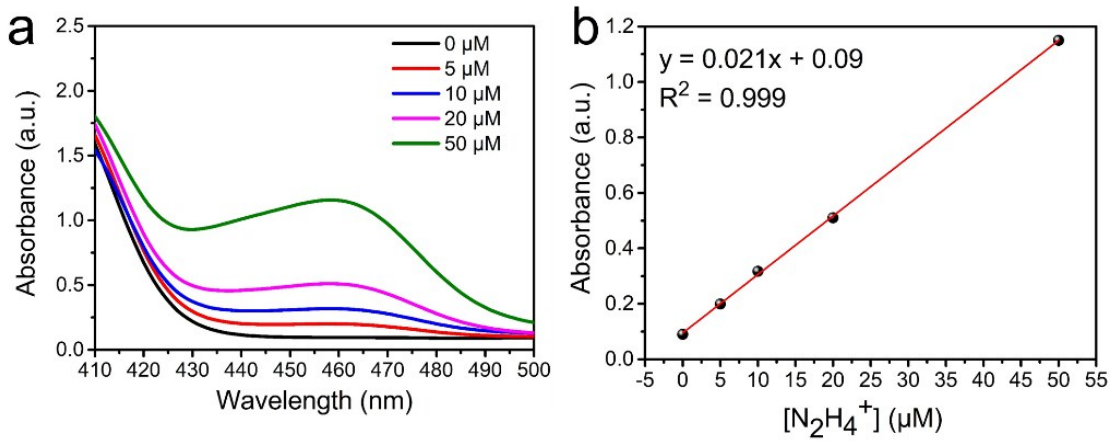

Fig. S5 (a) UV-Vis absorption spectra of various N2H4 concentrations after incubation for 20 min at room temperature. (b) Calibration curve used for calculation of N_2H_4 concentrations.

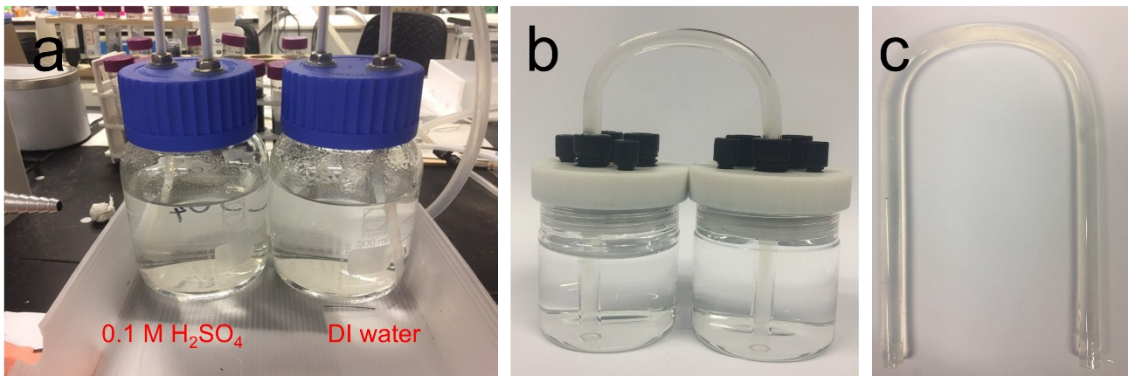

Fig. S6 Optical images of the (a) home-made filtration system, (b) electrochemical cell, (c) U-type salt bridge.

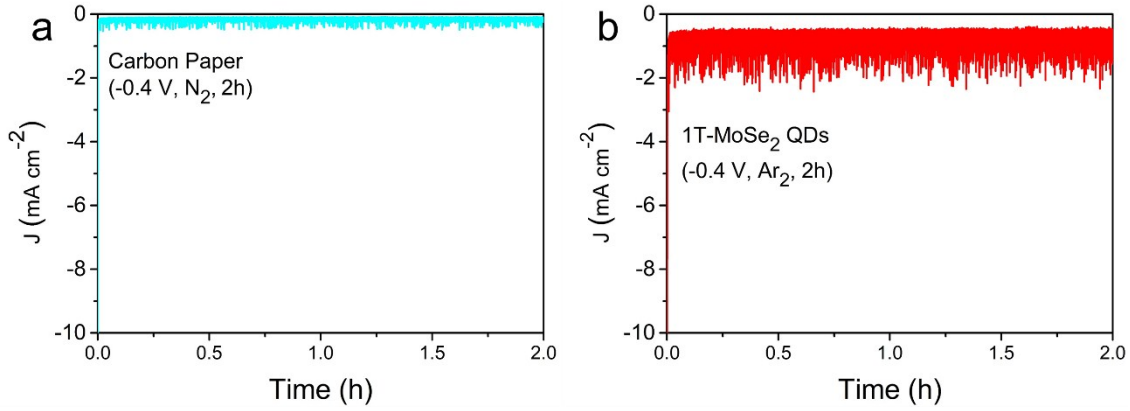

Fig. S7 (a) Chronoamperometry measurement of bare carbon paper electrode at the applied potential of -0.4 V in N_2-saturated 0.5 M Na_2SO_4 electrolyte. (b) Chronoamperometry measurements of 1T-$MoSe_2$ QDs electrode at the applied potential of -0.4 V in Ar_2-saturated 0.5 M Na_2SO_4 electrolyte.

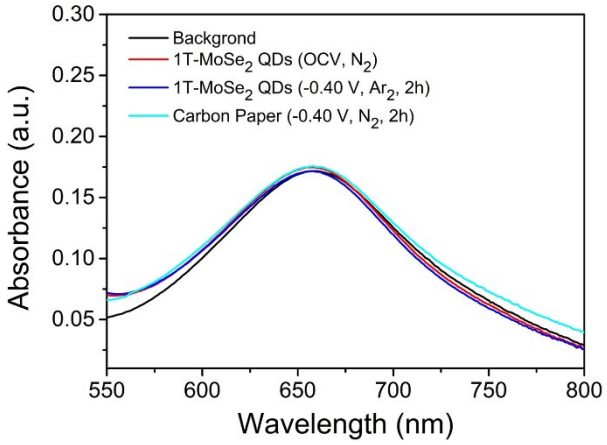

Fig. S8 UV-Vis absorption spectra of the electrolytes stained with indophenol indicator with no applied potential (OCV) in N_2-saturated electrolyte, bare carbon paper at the applied potential of -0.4 V in N_2-saturated electrolyte, and 1T-$MoSe_2$ QDs electrode at the applied potential of -0.4 V in Ar_2-saturated electrolyte.

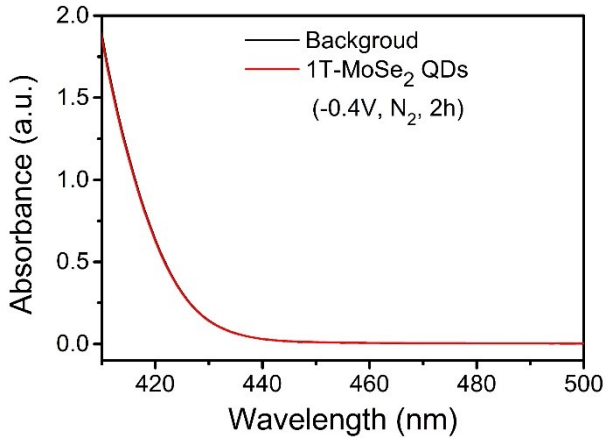

Fig. S9 UV-Vis absorption spectra of the electrolytes estimated by the method of Watt-Chrisp before and after 2 h electrolysis in N_2 atmosphere at the given potential of -0.4 V in N_2-saturated electrolyte using 1T-$MoSe_2$ QDs electrode.

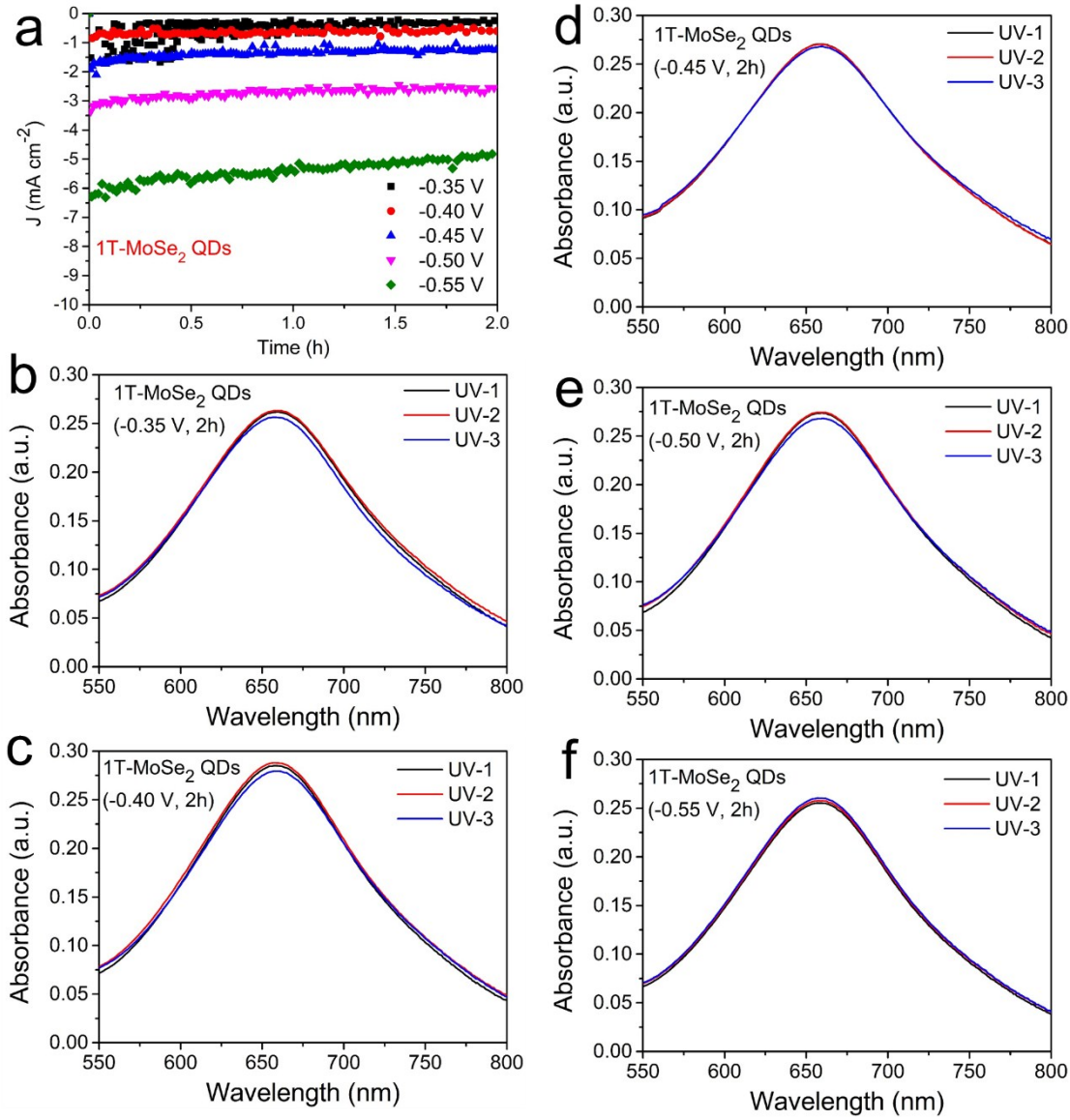

Fig. S10 (a) Chronoamperometry measurements of 1T-$MoSe_2$ QDs at different potentials N_2-saturated 0.5 M Na_2SO_4 electrolyte. (b-f) UV-Vis absorption spectra of the electrolytes stained with indophenol indicator after electrolysis at various potentials for 2 h.

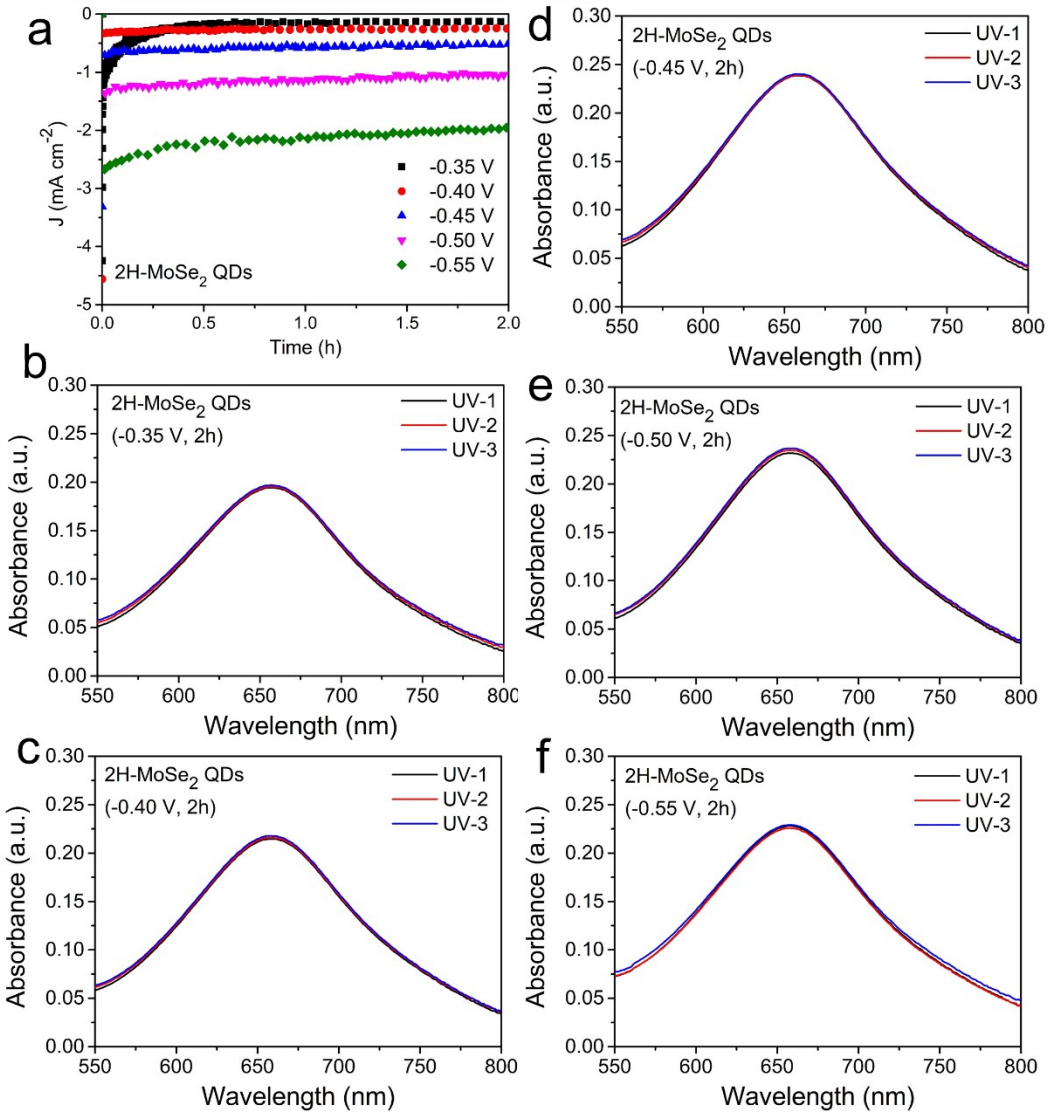

Fig. S11 (a) Chronoamperometry measurements of 2H-$MoSe_2$ QDs at different potentials N_2-saturated 0.5 M Na_2SO_4 electrolyte. (b-f) UV-Vis absorption spectra of the electrolytes stained with indophenol indicator after electrolysis at various potentials for 2 h.

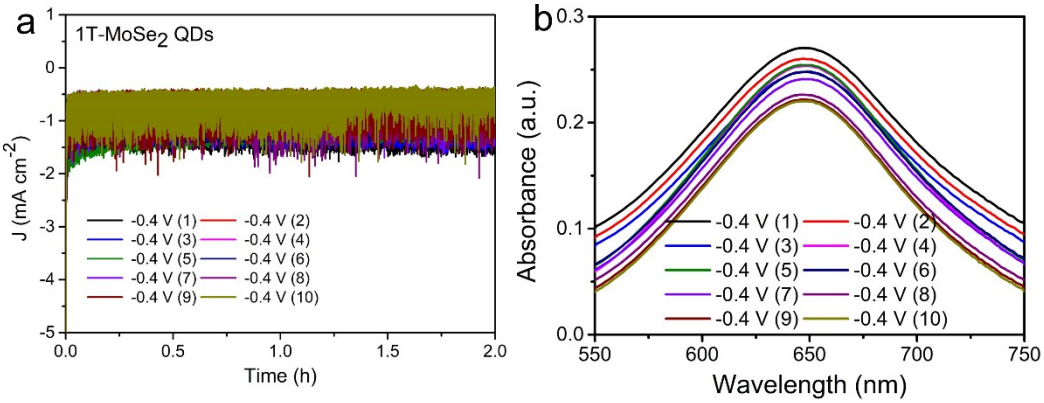

Fig. S12 (a) Chronoamperometry measurements of 1T-$MoSe_2$ QDs at the applied potential of -0.4 V in N_2-saturated 0.5 M Na_2SO_4 electrolyte. (b) The corresponded UV-Vis absorption spectra of the electrolytes stained with indophenol indicator.

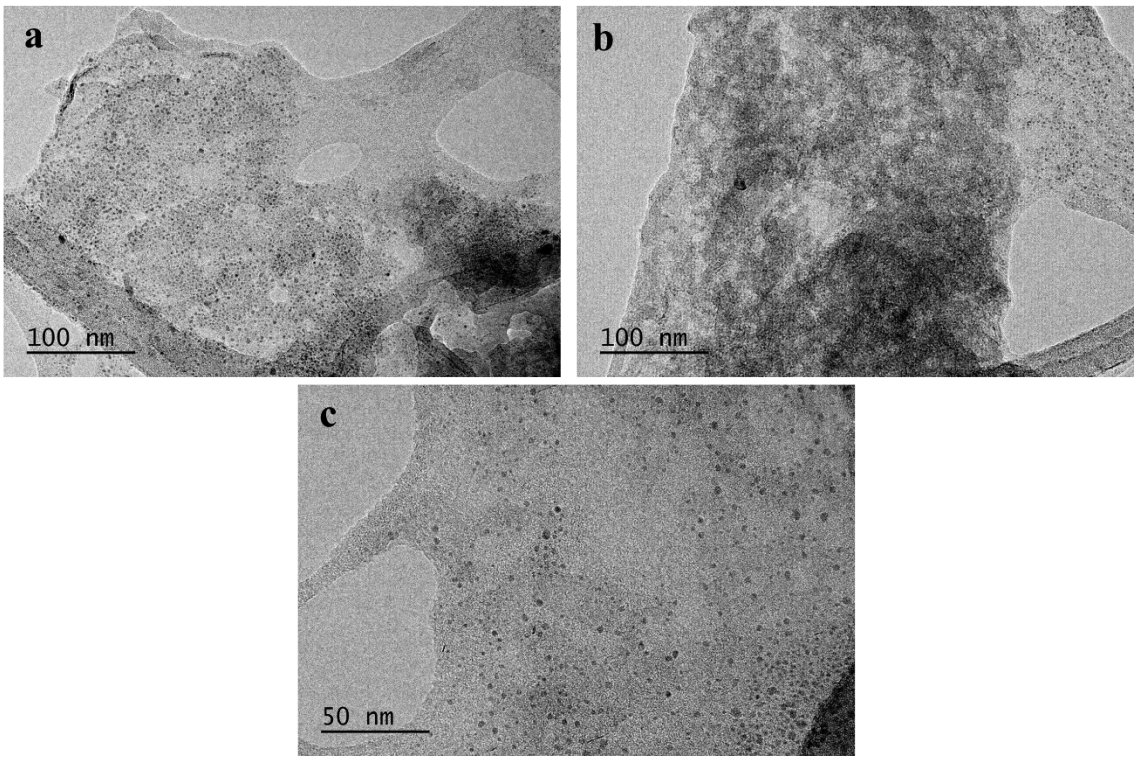

Fig. S13 TEM images of 1T-$MoSe_2$ QDs after ten NRR cycling tests.

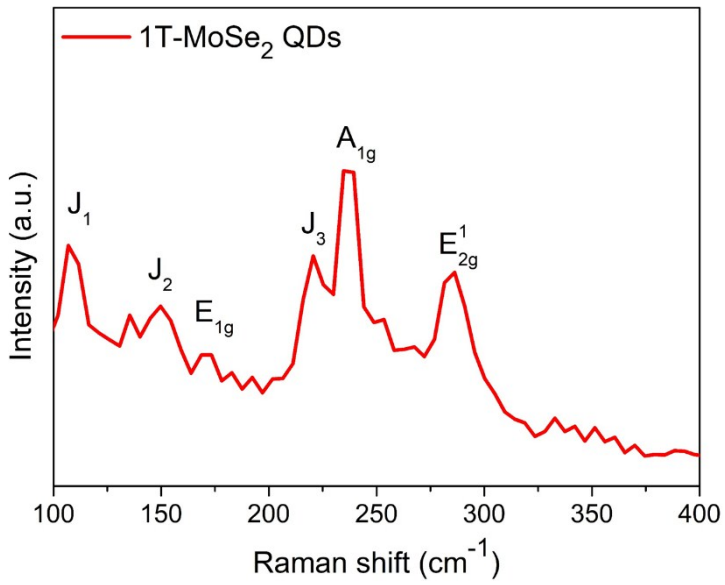

Fig. S14 Raman spectrum of 1T-$MoSe_2$ QDs after ten NRR cycling tests.

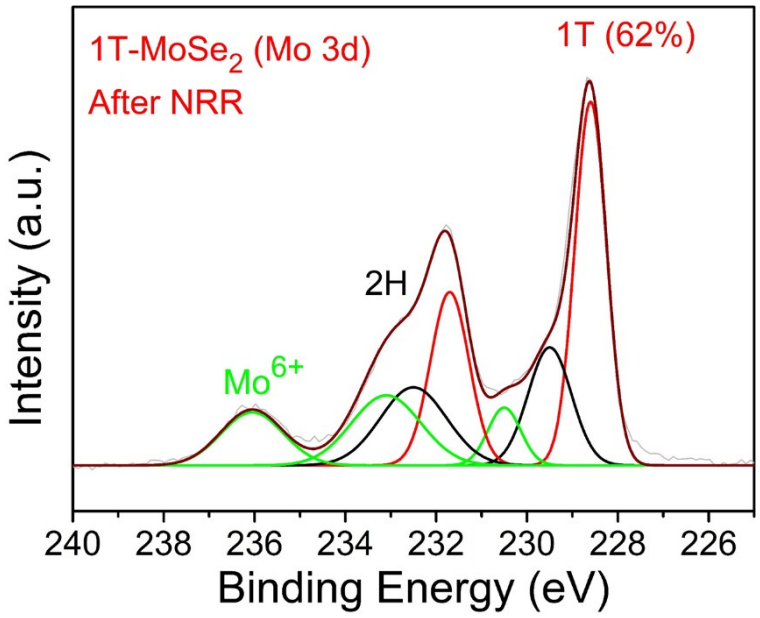

Fig. S15 The fitted Mo 3d XPS result of 1T-$MoSe_2$ QDs after ten NRR cycling tests.

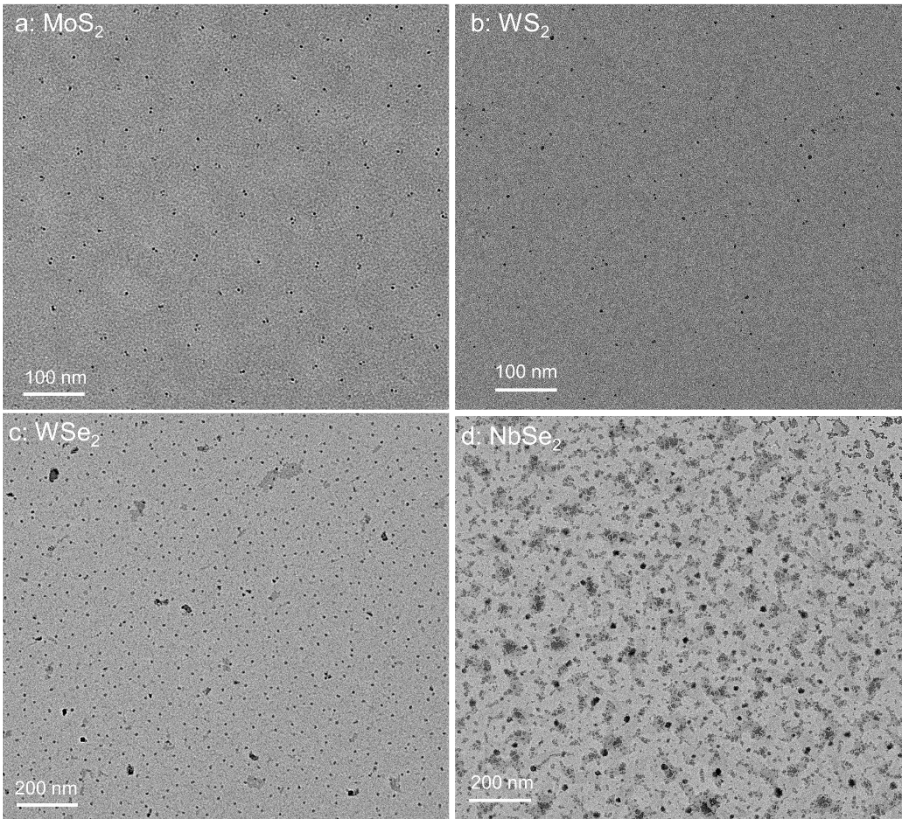

Fig. S16 TEM images of the as-prepared MoS_2, WSe_2, WS_2 and $NbSe_2$ QDs.

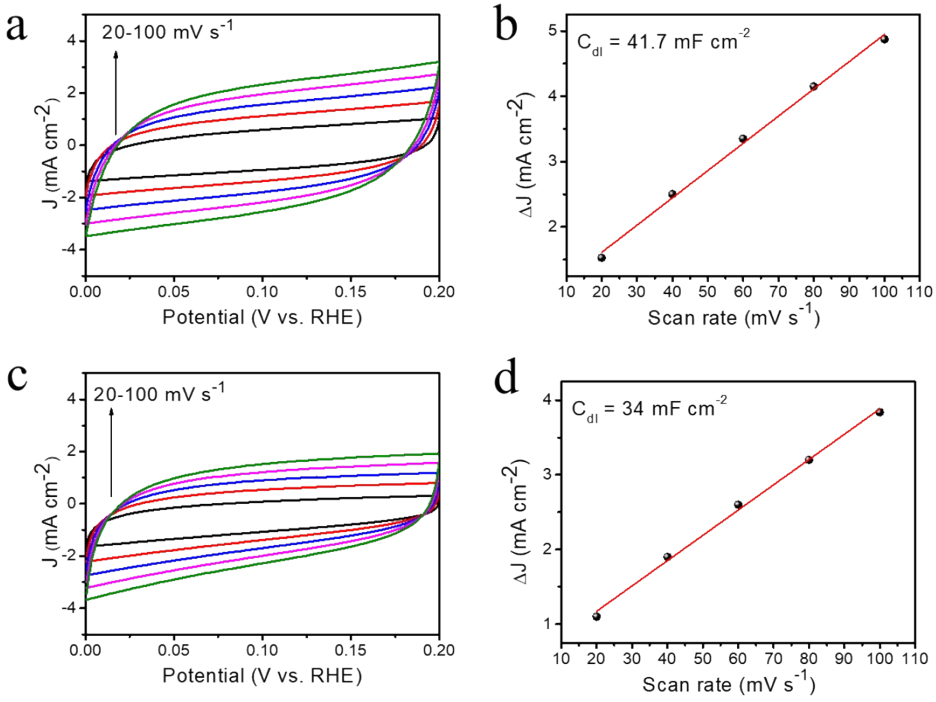

Fig. S17 CV curves and the extracted C_{dl} for (a,b) 1T- and (c,d) 2H- $MoSe_2$ QDs

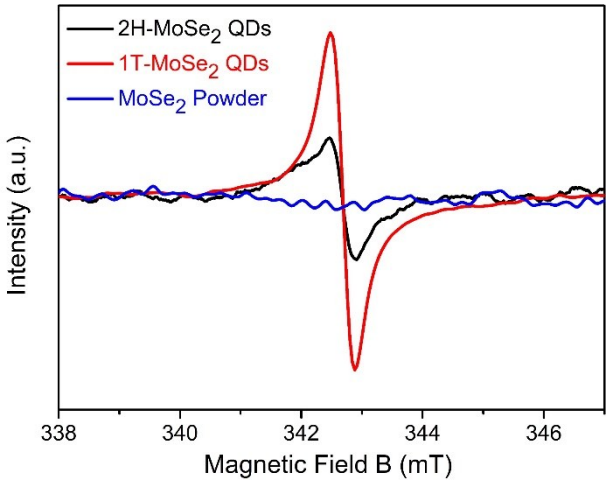

Fig. S18 EPR spectra of 1T- and 2H- $MoSe_2$ QDs, and 2H-$MoSe_2$ powder.

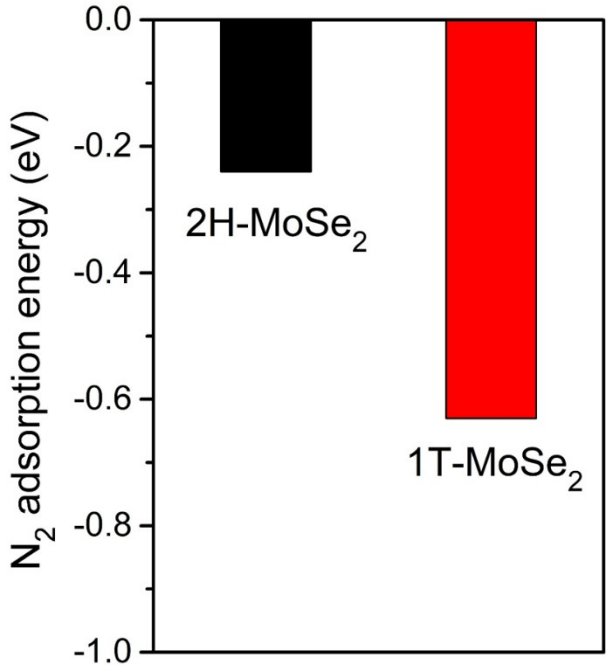

Fig. S19 N_2 adsorption energy of 1T- and 2H- $MoSe_2$ QDs

Table S1 Comparison of R_m on 1T-$MoSe_2$ QDs catalyst and other literature reported catalysts.

Catalyst	Rm (μg mg-1 cat. h^{-1})	Ref.
1T-$MoSe_2$ QDs	340	This work
a-Au/TiO_2	21.4	[5]
a-Au/CeO*x*–RGO	8.3	[6]
$Bi_4V_2O_{11}/CeO_2$	23.21	[7]
Rh nanosheets	23.88	[8]
Pd/C	4.5	[9]
Mo_2N nanorod	78.4	[10]
MoO_3 nanosheets	29.43	[11]
Ru SAs/N-C	120.9	[12]
Fe/Fe_3O_4	2.5	[13]
Nb_2O_5 nanofiber	43.6	[14]
Cr_2O_3 microspheres	25.3	[15]
FeMoS	8.45	[16]
Defect Bi	5.45	[17]
W_2N_3	12	[18]
BP	26.5	[19]
$La_2Ti_2O_7$	25.2	[20]
$K_2Ti_4O_9$	23	[21]
O-CNT	32	[22]
TiO_2+$Ti_3C_2T_x$	32	[23]
PdRu	37	[24]
F-C	9.3	[25]
FeNC	8.4	[26]
CoS_2/G	25	[27]
h-BN	18.2	[28]
Bi sheets	13.2	[29]
B nanosheets	3.1	[30]
Mo_2C	95	[31]

References

[1] X. Li, T. Li, Y. Ma, Q. Wei, W. Qiu, H. Guo, X. Shi, P. Zhang, A. M. Asiri, L. Chen, B. Tang, X. Sun, *Adv. Energy Mater.* **2018**, 1801357.

[2] G. Kresse, J. Furthmüller, *Phys. Rev. B* **1996**, 54, 11169; G. Kresse, D. Joubert, *Phys. Rev. B* **1999**, 59, 1758.

[3] P. E. Blöchl, *Phys. Rev. B* **1994**, 50, 17953.

[4] J. P. Perdew, J. Chevary, S. Vosko, K. A. Jackson, M. R. Pederson, D. Singh, C. Fiolhais, *Phys. Rev. B* **1992**, 46, 6671; J. P. Perdew, Y. Wang, *Phys. Rev. B* **1992**, 45, 13244.

[5] M. M. Shi, D. Bao, B. R. Wulan, Y. H. Li, Y. F. Zhang, J. M. Yan, Q. Jiang, *Adv. Mater.* **2017**, 29, 1606550.

[6] S. J. Li, D. Bao, M. M. Shi, B. R. Wulan, J. M. Yan, Q. Jiang, *Adv. Mater.* **2017** 29, 1700001.

[7] C. Lv, C. Yan, G. Chen, Y. Ding, J. Sun, Y. Zhou, G. Yu, *Angewandte Chemie* **2018**, 57, 6073.

[8] H.-M. Liu, S.-H. Han, Y. Zhao, Y.-Y. Zhu, X.-L. Tian, J.-H. Zeng, J.-X. Jiang, B. Y. Xia, Y. Chen, *J. Mater. Chem. A* **2018**, 6, 3211.

[9] J. Wang, L. Yu, L. Hu, G. Chen, H. Xin, X. Feng, *Nat. Commun.* **2018**, 9, 1795.

[10] X. Ren, G. Cui, L. Chen, F. Xie, Q. Wei, Z. Tian, X. Sun, *Chem Commun (Camb)* **2018**, 54, 8474.

[11] J. Han, X. Ji, X. Ren, G. Cui, L. Li, F. Xie, H. Wang, B. Li, X. Sun, *J. Mater. Chem. A* **2018** 6, 12974.

[12] Z. Geng, Y. Liu, X. Kong, P. Li, K. Li, Z. Liu, J. Du, M. Shu, R. Si, J. Zeng, *Adv. Mater.* **2018**, e1803498.

[13] L. Hu, A. Khaniya, J. Wang, G. Chen, W. E. Kaden, X. Feng, *ACS Catal.* **2018**, 9312.

[14] J. Han, Z. Liu, Y. Ma, G. Cui, F. Xie, F. Wang, Y. Wu, S. Gao, Y. Xu, X. Sun, *Nano Energy* **2018**, 52, 264.

[15] Y. Zhang, W. Qiu, Y. Ma, Y. Luo, Z. Tian, G. Cui, F. Xie, L. Chen, T. Li, X. Sun, *ACS Catal.* **2018** 8, 8540.

[16] Y. Guo, Z. Yao, B. J. J. Timmer, X. Sheng, L. Fan, Y. Li, F. Zhang, L. Sun, *Nano Energy* **2019**, 62, 282.

[17] Y. Wang, M. M. Shi, D. Bao, F. L. Meng, Q. Zhang, Y. T. Zhou, K. H. Liu, Y. Zhang, J. Z. Wang, Z. W. Chen, D. P. Liu, Z. Jiang, M. Luo, L. Gu, Q. H. Zhang, X. Z. Cao, Y. Yao, M. H. Shao, Y. Zhang, X. B. Zhang, J. G. Chen, J. M. Yan, Q. Jiang, *Angewandte Chemie* **2019** .

[18] H. Jin, L. Li, X. Liu, C. Tang, W. Xu, S. Chen, L. Song, Y. Zheng, S. Z. Qiao, *Adv. Mater.* **2019** **2D**, e1902709.

[19] X. Zhu, T. Wu, L. Ji, C. Li, T. Wang, S. Wen, S. Gao, X. Shi, Y. Luo, Q. Peng, X. Sun, *J. Mater. Chem. A* **2019**.

[20] J. Yu, C. Li, B. Li, X. Zhu, R. Zhang, L. Ji, D. Tang, A. M. Asiri, X. Sun, Q. Li, S. Liu, Y. Luo, *Chem Commun* **2019**, 55, 6401.

[21] D. Wu, H. Wang, H. Huang, R. Zhang, L. Ji, H. Chen, Y. Luo, J. You, D. Tang, Z. Zhang, X. Sun, *Chem Commun* **2019**, 55, 7546.

[22] J. Zhao, B. Wang, Q. Zhou, H. Wang, X. Li, H. Chen, Q. Wei, D. Wu, Y. Luo, J. You, F. F. Gong, X. Sun, *Chem Commun* **2019**.

[23] Y. Fang, Z. Liu, J. Han, Z. Jin, Y. Han, F. Wang, Y. Niu, Y. Wu, Y. Xu, *Adv. Energy Mater.* **2019** 1803406.

[24] H. Wang, Y. Li, C. Li, K. Deng, Z. Wang, Y. Xu, X. Li, H. Xue, L. Wang, *J. Mater. Chem. A* **2019**, 7, 801.

[25] J. Zhao, J. Yang, L. Ji, H. Wang, H. Chen, Z. Niu, Q. Liu, T. Li, G. Cui, X. Sun, *Chem Commun (Camb)* **2019**, 55, 4266.

[26] M. Wang, S. Liu, T. Qian, J. Liu, J. Zhou, H. Ji, J. Xiong, J. Zhong, C. Yan, *Nat. Commun.* **2019**, 10.

[27] P. Chen, N. Zhang, S. Wang, T. Zhou, Y. Tong, C. Ao, W. Yan, L. Zhang, W. Chu, C. Wu, Y. Xie, *Proceedings of the National Academy of Sciences of the United States of America* **2019**, 116, 6635.

[28] J. Zhao, X. Ren, X. Li, D. Fan, X. Sun, H. Ma, Q. Wei, D. Wu, *Nanoscale* **2019**, 11, 4231.

[29] L. Li, C. Tang, B. Xia, H. Jin, Y. Zheng, S.-Z. Qiao, *ACS Catal.*, 9, 2902.

[30] Q. Fan, C. Choi, C. Yan, Y. Liu, J. Qiu, S. Hong, Y. Jung, Z. Sun, *Chem Commun (Camb)* **2019**, 55, 4246.

[31] X. Ren, J. Zhao, Q. Wei, Y. Ma, H. Guo, Q. Liu, Y. Wang, G. Cui, A. M. Asiri, B. Li, B. Tang, X. Sun, *ACS Cent. Sci.* **2019** 5, 116.